Ore Geology Reviews 74 (2016) 88–100

Contents lists available at ScienceDirect

Ore Geology Reviews

journal homepage: www.elsevier.com/locate/oregeorev

Geological and isotopic constraints on the origin of the Anle carbonate-hosted Zn–Pb deposit in northwestern Yunnan Province, SW China

Jia-Xi Zhou [a,*], Kai Luo [a,b], Bo Li [c], Zhi-Long Huang [a], Zai-Fei Yan [a]

[a] State Key Laboratory of Ore Deposit Geochemistry, Institute of Geochemistry, Chinese Academy of Sciences, Guiyang 550081, China
[b] University of Chinese Academy of Sciences, Beijing 100049, China
[c] Faculty of Land Resource and Engineering, Kunming University of Science and Technology, Kunming 650093, China

ARTICLE INFO

Article history:
Received 17 July 2015
Received in revised form 10 November 2015
Accepted 12 November 2015
Available online 14 November 2015

Keywords:
C–O–S–Zn and Pb isotopes
Ore-forming fluids and metals
Anle Zn–Pb deposit
Songpan–Ganzi Block
Southwest China

ABSTRACT

The Anle Zn–Pb deposit, hosted by Upper Cambrian dolostone, is located in the southern Songpan–Ganzi Block in southwest China. In this deposit, ore bodies occur as stratiform lenses and consist of galena, sphalerite and pyrite as ore minerals, and quartz, dolomite and calcite as gangue minerals. The mineralization shows mainly vein, banded and brecciated structures. Four ore bodies have been found in the Anle deposit, with a combined 2.0 million tonnes (Mt) of sulfide ores at average grades of 1.64 wt.% Pb, 6.64 wt.% Zn and 45 g/t Ag. Brown, brownish-yellow and yellow sphalerite samples have $\delta^{66}Zn$ values ranging from +0.08 to +0.10‰ (average + 0.09‰, $n = 3$), +0.12 to +0.38‰ (average + 0.24‰, $n = 8$) and +0.40 to +0.50‰ (average + 0.46‰, $n = 3$), respectively. We interpret the progressively heavier Zn isotopes from brown to yellow sphalerite as being led by kinetic Raleigh fractional crystallization. Calcite samples have $\delta^{13}C_{PDB}$ and $\delta^{18}O_{SMOW}$ values ranging from −4.8 to −0.2‰ (average −1.7‰, $n = 7$) and +17.9 to +21.4‰ (average +19.6‰, $n = 7$), respectively. Whole-rock $\delta^{13}C_{PDB}$ and $\delta^{18}O_{SMOW}$ values of the Cambrian ore-hosting dolostone range from +0.1 to +1.1‰ (average +0.6‰, $n = 3$) and +23.2 to +24.1‰ (average +23.6‰, $n = 3$), respectively. This suggests that carbon in the ore-forming fluids was provided by the host dolostone through carbonate dissolution. $\delta^{34}S_{CDT}$ values of sulfide samples range between −1.3‰ and +17.8‰ with an average value of +6.3‰ ($n = 25$), lower than evaporites (such as barite +19.8‰) in the overlaying Lower Ordovician sedimentary strata. The data suggest that sulfur in the hydrothermal fluids were derived from evaporites by thermo-chemical sulfate reduction (TSR). $^{206}Pb/^{204}Pb$, $^{207}Pb/^{204}Pb$ and $^{208}Pb/^{204}Pb$ ratios for sulfide minerals range from 17.63 to 17.86, 15.58 to 15.69 and 37.62 to 37.95, respectively. The data are similar to those of the age-corrected Cambrian ore-hosting dolostone ($^{206}Pb/^{204}Pb = 17.70–17.98$, $^{207}Pb/^{204}Pb = 15.58–15.65$ and $^{208}Pb/^{204}Pb = 37.67–38.06$), but lower than those of age-corrected Ordovician sandstone and slate ($^{206}Pb/^{204}Pb = 18.54–19.58$, $^{207}Pb/^{204}Pb = 15.73–15.81$ and $^{208}Pb/^{204}Pb = 38.44–39.60$). This indicates that ore Pb was most likely to be derived from the Cambrian ore-hosting dolostone. Therefore, our new geological and isotopic evidence suggests that the Anle Zn–Pb deposit is best classified to be an epigenetic carbonate-hosted Mississippi Valley-type (MVT) deposit.

1. Introduction

The Sanjiang (three rivers in Chinese: Jinshajiang, Lancangjiang and Nujiang) tectonic belt in southwestern China, extending for more than 1500 km, is an important polymetallic metallogenic belt with abundant Cu–Mo–(Au) and Pb–Zn–Ag deposits in the Eastern India–Eurasia collision zone (e.g., Hou et al., 2007; Hou and Cook, 2009). The Anle Zn–Pb deposit is located in the eastern section of the Songpan–Ganzi Block, in the mid-northern part of the Sanjiang metallogenic belt (Fig. 1A). The Songpan–Ganzi Block is situated between the Yangtze Block to the east and the Lanping–Simao basin to the west (Fig. 1A). Studies indicate that the main deformation process of the Songpan–Ganzi fold belt occurred during the Late Triassic (e.g., Chang, 2000; Xu et al., 1992). More than 400 carbonate-hosted Pb–Zn deposits have been found in the western Yangtze Block (Liu and Lin, 1999), and they constitute the famous Sichuan–Yunnan–Guizhou (SYG) Pb–Zn metallogenic province (Huang et al., 2010; Zhou et al., 2013a, 2014a, 2015). Among these deposits, there are many large scale (>1 Mt Pb + Zn metal reserves) Pb–Zn deposits, such as the Huize Zn–Pb–Ge (Han et al., 2007; Huang et al., 2010; Zhou et al., 2001), Daliangzi Zn–Pb–Cd (Zheng and Wang, 1991) and Tianbaoshan Zn–Pb deposits (Zhou et al., 2013b). There are also many famous sediment-hosted Pb–Zn deposits in the Lanping–Simao basin, including the world-class (>10 Mt Pb + Zn) Jinding Pb–Zn deposit (Tang et al., 2014; Xue et al., 2007) and the large scale Baiyangping Pb–Zn deposit (Zhang et al., 2013). However,

* Corresponding author.
E-mail address: zhoujiaxi@vip.gyig.ac.cn (J.-X. Zhou).

http://dx.doi.org/10.1016/j.oregeorev.2015.11.019
0169-1368/

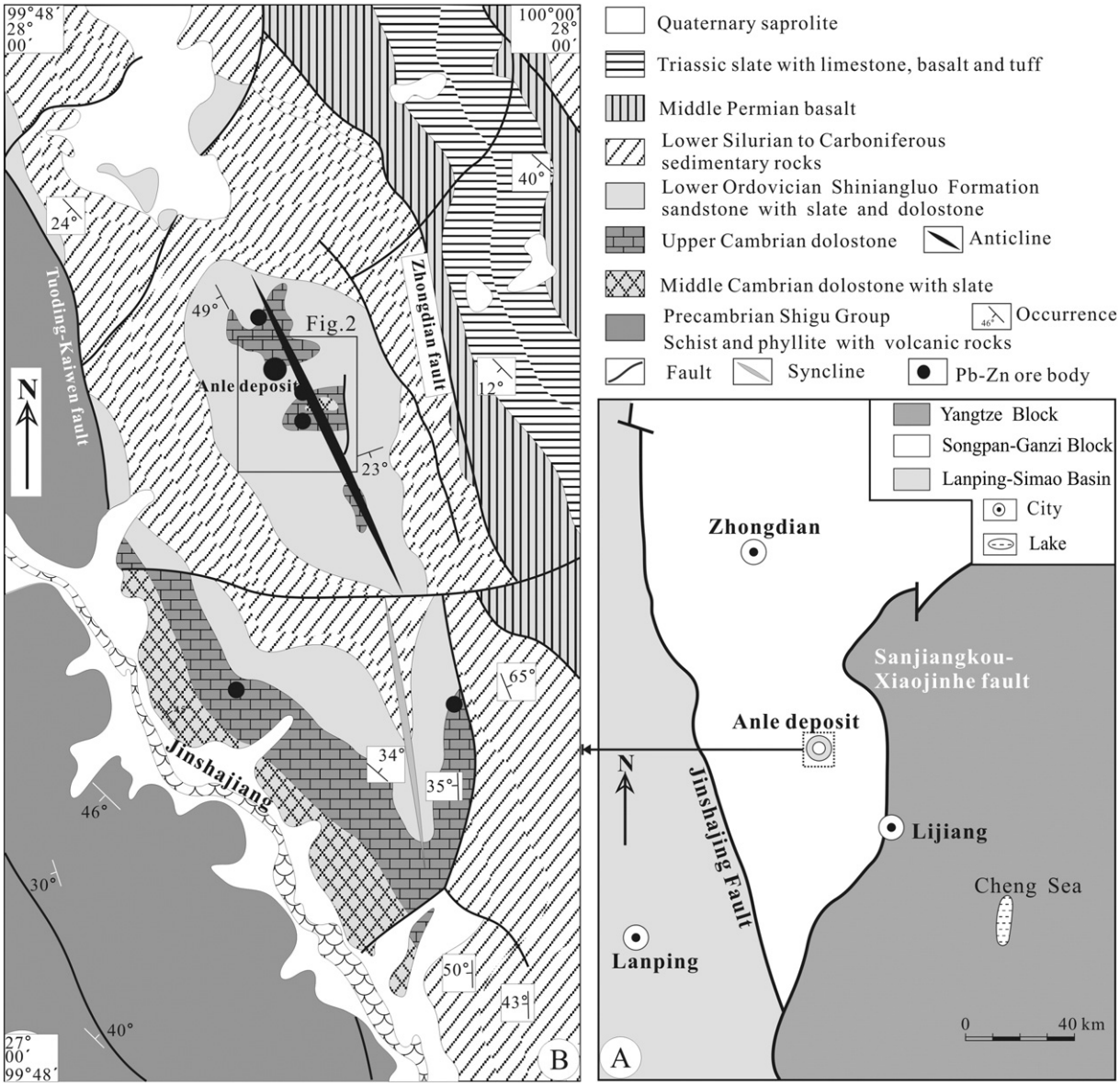

Fig. 1. A: Map showing the tectonic setting of the Anle Zn–Pb deposit district; B: Regional map of the Anle Zn–Pb deposit showing faults, folds, lithologies and deposits. Modified from Wang et al. (2011).

in the southern part of the Songpan–Ganzi Block, no large scale sediment-hosted Pb–Zn deposits were reported (Wang et al., 2011).

The Anle Zn–Pb deposit has been mined since 1736 AD (the Qing dynasty Qianlong Period), and by then extraction of Ag was given priority over other metals. This deposit contains more than 2.0 Mt of sulfide ores with an average grade of 1.64 wt.% Pb, 6.64 wt.% Zn and 45 g/t Ag (Wang et al., 2011). Ore deposit geology and fluid inclusion geochemistry indicate that the Anle Pb–Zn deposit is different from many Zn–Pb deposits in the western Yangtze Block (SYG-type, Li et al., 2015; Zhou et al., 2013c, 2014b) and the Lanping–Simao basin (Jinding-type, Tang et al., 2014; Wang et al., 2014; Xue et al., 2007), but similar to other carbonate-hosted Pb–Zn deposits (Mississippi Valley-type) in the southern Songpan–Ganzi Block (Wang et al., 2011), as evidenced by: (i) ore bodies are hosted in Upper Cambrian dolostone, (ii) Zn–Pb mineralization occurs within the Anle anticline, (iii) simple mineral assemblage and wall rock alteration, (iv) evaporites are common in Lower Ordovician Shiniangluo Formation sandstone, (v) organic matter is abundant in Middle Cambrian shale, and (vi) ore-forming fluids have medium–high temperatures (130–370 °C) and low salinities (3.0–12.8 wt.% eq. NaCl). However, despite the fluid inclusion geochemical work done by Wang et al. (2011), there are still many unknown aspects regarding the source of ore-forming fluids and metals, ore genesis and geodynamic setting of the Anle Zn–Pb deposit.

C–O and S isotopes have been widely used to constrain the source of the ore-forming fluids (e.g., Basuki et al., 2008; Huang et al., 2003, 2010; Ohmoto and Goldhaber, 1997; Palinkaš et al., 2013; Pašava et al., 2014; Zhou et al., 2013d, 2014b), and Pb isotopes are useful for tracing the origin of the ore-forming metals for carbonate-hosted sulfide deposits (e.g., Carr et al., 1995; Gromek et al., 2012; Mirnejad et al., 2011; Pass et al., 2014; Xue et al., 2007; Zhou et al., 2013e, 2016). In addition, Zn isotopes have recently been used for understanding the geochemical process of Zn extraction, transportation and deposition in hydrothermal systems (e.g., Chen et al., 2013; Fujii et al., 2011; Gagnevin et al., 2012; John et al., 2008; Kelley et al., 2009; Mason et al., 2005; Pašava et al., 2014; Toutain et al., 2008; Wilkinson et al., 2005; Zhou et al., 2014a, 2014b). In this paper, we describe the Anle Zn–Pb ore deposit geology and report new C–O isotopic data of hydrothermal calcite and the ore-hosting dolostone whole-rock, S- and Zn isotopic data of sulfide minerals, and Pb isotopic data of wall rocks and sulfides. This new dataset, together with the previously published data of fluid inclusions in

hydrothermal quartz (Wang et al., 2011), are used to understand the source of the ore-forming fluids and metals and the ore-forming process of the Anle Zn–Pb deposit. These results are also used to discuss the causes of the fractionation of Zn isotopes during Pb–Zn mineralization.

2. Regional geology

The Songpan–Ganzi Block is bounded by the Yangtze Block to the east and the Sanjiang fold belt to the west (Fig. 1A). In the southern Songpan–Ganzi Block, the Precambrian Shigu Group represents the Proterozoic basement (Fig. 1B), which consists of schist, phyllite and volcanic rocks. These rocks are unconformably overlain by shallow marine Paleozoic and Lower Mesozoic sequence (Fig. 1B). The Cambrian strata are composed of dolostone interbedded with slate. The overlying Ordovician sequence consists of sandstone inter-bedded with dolostone and slate, which in turn, are overlain by Silurian limestone and dolostone inter-bedded with sandstone. Devonian rocks, including slate, sandstone, limestone and dolostone, are overlain by Carboniferous limestone. Permian rocks include basalts, whereas Triassic rocks include slate inter-bedded with limestone, basalt and tuff (Fig. 1B). It is worth mentioning that the Middle Permian Emeishan large igneous province (LIP) flood basalts (ca. 260 Ma; Zhou et al., 2002) occur in the southern Songpan–Ganzi Block. Evaporites and carbonaceous sediments are common in the Cambrian to Triassic strata (Wang et al., 2011). Cenozoic rocks are composed entirely of terrigenous sediments. Major structures consist of NW-trending faults and folds, such as the Tuoding–Kaiwen and Zhongdian faults and the Anle anticline, whereas younger NE- or EW-trending faults crosscut these major structures (Fig. 1B). The Anle Zn–Pb deposit occurs in the NW-limb of the Anle anticline and is hosted by Upper Cambrian dolostone. The deposit is the largest carbonate-hosted Pb–Zn deposit in the southern Songpan–Ganzi Block, Shangri-La County, northwestern Yunnan Province (Fig. 1B).

3. Geology of the Anle deposit

3.1. Stratigraphy

In the Anle Zn–Pb deposit area, the exposed strata include Middle to Upper Cambrian and Lower Ordovician sedimentary rocks, and Quaternary colluviums (Fig. 2). Middle Cambrian rocks mainly consist of dolostone inter-layered with slate, and are overlain by Upper Cambrian dolostone. Overlying the Upper Cambrian rocks are slate and sandstone of the Lower Ordovician Shiniangluo Formation. The Shiniangluo Formation can be divided into two sections: Slate in the lower section and sandstone in the upper section. Zn–Pb–Ag mineralization in the Anle deposit is hosted by Upper Cambrian dolostone (Figs. 2 and 3). The Quaternary sediments consist of sand, gravel and clay.

3.2. Structure

Folded Middle–Upper Cambrian and Lower Ordovician sedimentary rocks form the NW-trending Anle anticline (Fig. 2). The Middle Cambrian dolostone and slate occur at the core of the Anle anticline, and the Upper Cambrian and Lower Ordovician dolostone, slate and sandstone form the flanks. This anticline extends for 7 km in length and is about 4 km wide. The limbs of the Anle anticline dip between 20° and 22° in the northeast, and from 40° to 48° in the southwest. Major faults in the Anle deposit are not developed and only a few small faults in the Eastern District are present (Fig. 2). The Anle deposit is associated with the Anle anticline and occurs in its southwestern wing (Fig. 3).

3.3. Ore bodies

Four ore bodies occurring as strata-bound lenses have been found in the Anle deposit (Wang et al., 2011), of which I and II ore bodies are the

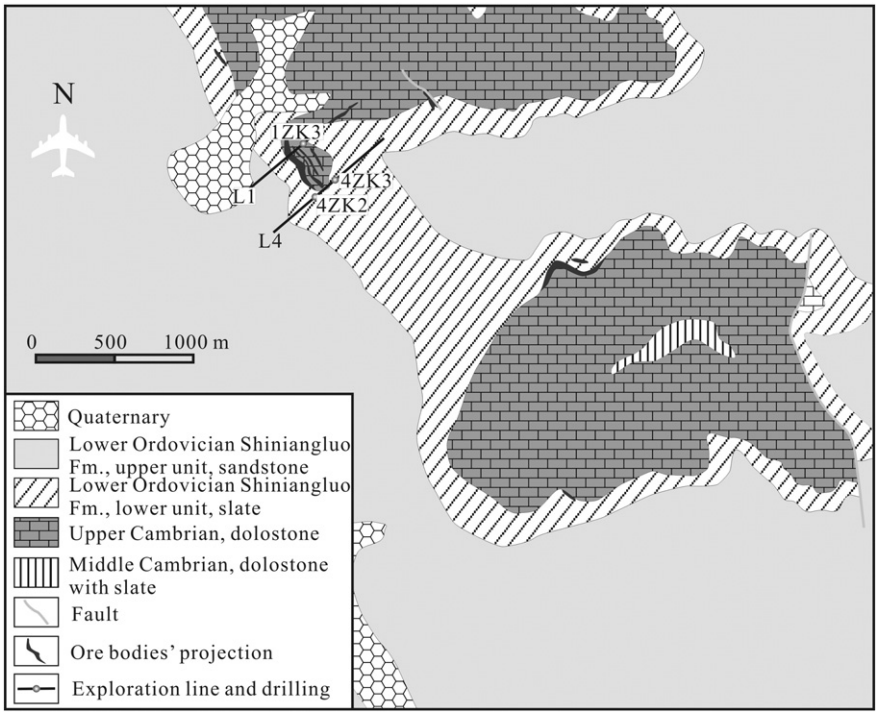

Fig. 2. Geological map of the Anle Zn–Pb deposit showing the lithologies, faults, folds, exploration lines and projections of ore bodies. Modified from Wang et al. (2011).

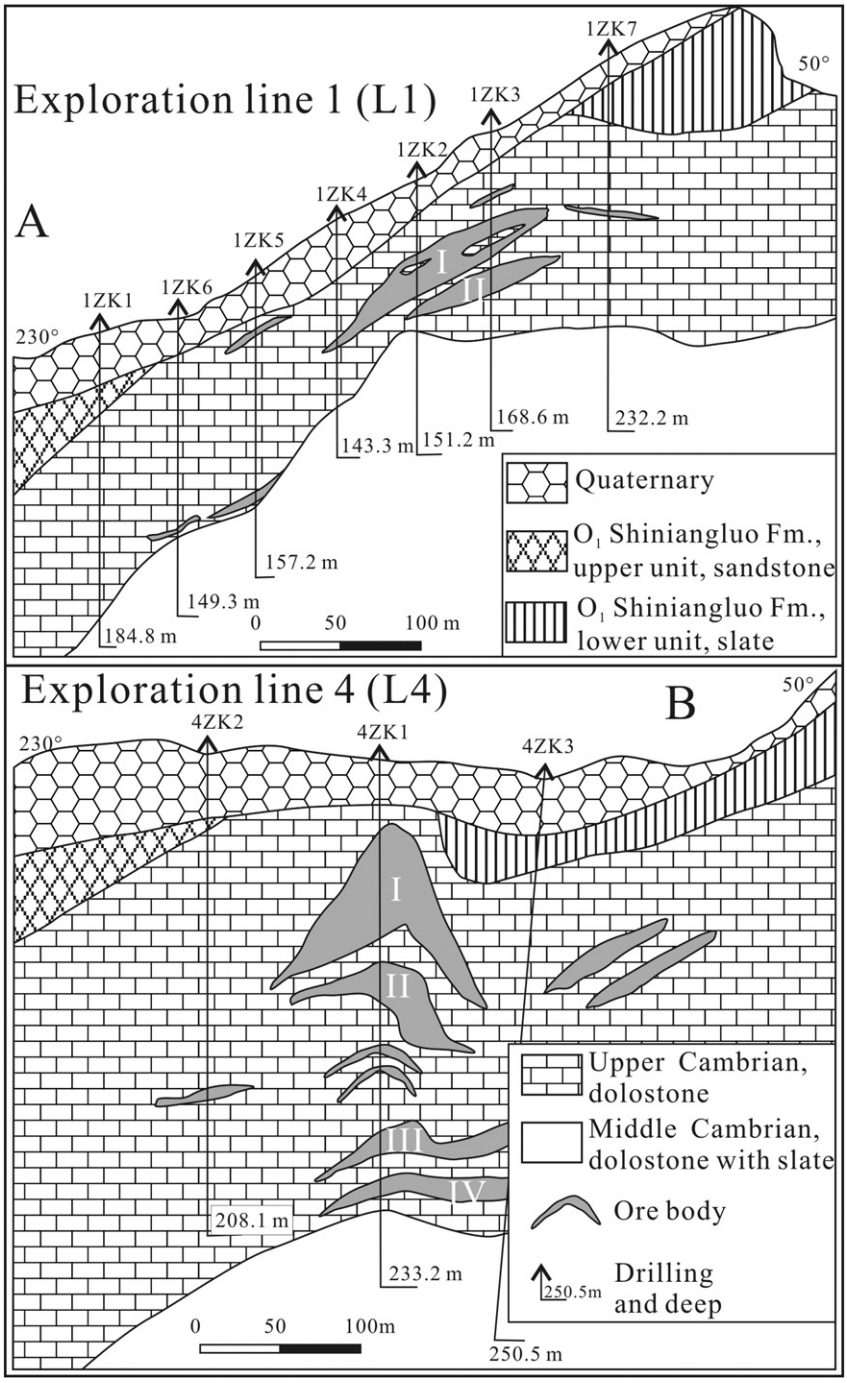

Fig. 3. Exploration lines L1 (A) and L4 (B) cross-sections of the Anle Zn–Pb deposit showing the drilling, ore bodies and host rock lithologies. Modified from Wang et al. (2011).

two largest (Figs. 2 and 3). Ore body I occurs in Upper Cambrian dolostone between 2555 m and 2650 m levels. This ore body is 500 m long, 165 m wide and 2.3 m to 30.6 m thick with dip angles between 36° and 51°, and contains 0.97 Mt of sulfide ore at grades of 0.59 to 4.81 wt.% (average 1.64 wt.%) Pb, 3.68 to 11.65 wt.% (average 6.64 wt.%) Zn, and 5 to 155 g/t (average 55 g/t) Ag. Ore body II also occurs in the Upper Cambrian dolostone, but at 2560 m to 2730 m levels. This ore body is 560 m in length, 150 m in depth and 1.89 m to 32.2 m in thickness with dip angles from 50° to 56°, and contains 1.22 Mt of sulfide ore at grades of 0.09 to 1.99 wt.% (average 0.95 wt.%) Pb, 2.04 to 10.56 wt.% (average 5.11 wt.%) Zn, and 2 to 105 g/t (average 35 g/t) Ag.

3.4. Texture and structure

Ore minerals mainly consist of galena, sphalerite and pyrite. Gangue minerals include mainly quartz and calcite. These minerals formed simple mineral assemblages, including sphalerite + galena + quartz ± calcite (Fig. 4A, E, F, I) and pyrite + sphalerite + galena + calcite ± dolomite (Fig. 4B, C, D, G, H, J, K, L). Ores have mainly vein (Fig. 4A, B,

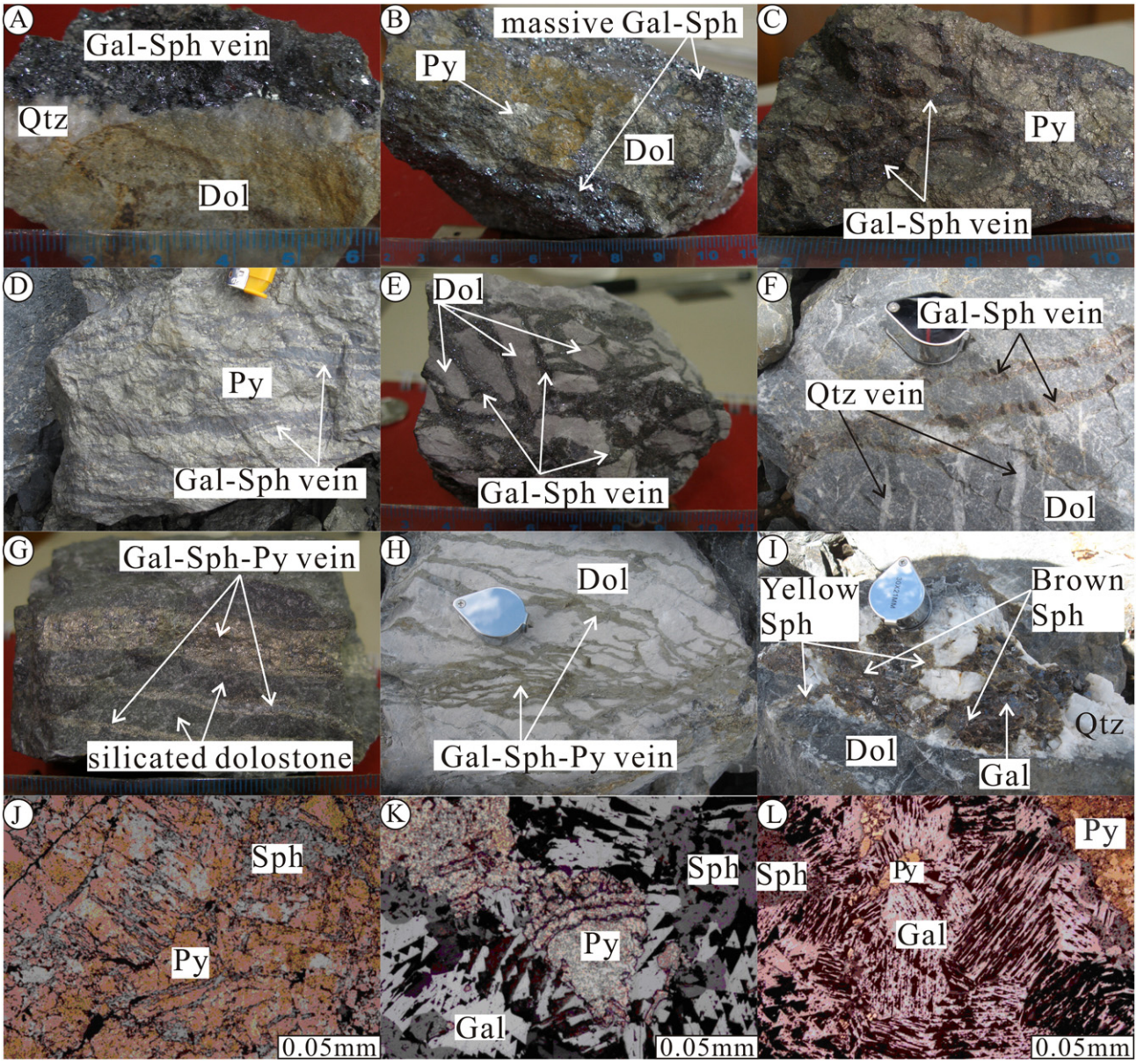

Fig. 4. Mineral assemblage and textures of sulfide ore in the Anle Zn–Pb deposit. A: quartz (Qtz) situated between sphalerite (Sph)–galena (Gal) vein and dolostone (Dol); B: disseminate pyrite (Py) in residual Dol that is enclosed in massive Sph–Gal aggregate; C: Pb–Zn vein in massive Py aggregate; D: Sph–Gal veinlet in massive Py aggregate; E: Sph–Gal vein filling in brecciated Dol; F: Sph–Gal vein and Qtz vein in Dol. G: Sph–Gal–Py vein in silicate dolostone; H: Sph–Gal–Py vein in Dol; I: Sph coexisting with Gal and Qtz occurring as veined aggregate in Dol; J: metasomatic Sph in Py; K: eutectic boundaries among Sph, Py and Gal; L: early stage Py enclosed in pressure shadow Gal that coexist with late stage Py and Sph.

C, D, F, H), banded (Fig. 4G) and brecciated (Fig. 4E, I) structures, and metasomatic (Fig. 4J), annealing boundary (Fig. 4K), and pressure shadow (Fig. 4L) textures. Different minerals show various textures and structures in different ores. For example, in banded ores (Fig. 4G), galena forms aggregates of fine-grained (0.03–0.10 mm) anhedral crystals (Fig. 4K). Sphalerite is enclosed in galena with anhedral crystal (Fig. 4K). In brecciated ores, galena forms aggregate of fine-grained (0.01–0.04 mm) euhedral crystals (Fig. 4L). In many places, sphalerite co-exists with euhedral galena (Fig. 4L). In addition, similar to other carbonate-hosted Zn–Pb deposits in southwest China, sphalerite in the Anle deposit also shows three main colors due to varying contents of minor elements (such as Fe and Cd) (e.g., Ye et al., 2011; Zhou et al., 2014a), including brown, brownish-yellow and yellow (Fig. 4I). Brown sphalerite often formed in the early stage at relatively high temperatures, and has high contents of Fe and other elements as ionic substitution of Zn, while yellow sphalerite commonly precipitated in the final stage at relatively low temperatures with lower contents of other elements than Zn (e.g., Pašava et al., 2014; Ye et al., 2011; Zhou et al., 2014a).

3.5. Mineral paragenesis

Ore-forming processes of the Anle Zn–Pb deposit include hydrothermal and supergene oxidizing two stages. Based on crosscutting, overgrowth and replacement relationships, the hydrothermal stage is divided into the sulfide + quartz + calcite and the quartz + calcite ± dolomite sub-stages. The former sub-stage is the main economic stage and has ore mineral assemblages of sphalerite + galena and pyrite + sphalerite + galena (Fig. 4). Sphalerite has variable colors, including brown, brownish-yellow and yellow (Fig. 4I). In general, brown sphalerite formed earlier than yellow sphalerite (e.g., Ye et al., 2011; Zhou et al., 2014a), whereas brownish-yellow sphalerite can be formed during the entire sulfide mineralization process. In the Anle deposit, yellow sphalerite always occurs as vein and distributes along the boundary

Table 1
Mineral paragenesis of the Anle Zn-Pb deposit.

Period	Hydrothermal		Supergene
Stage	Sulfide + quartz + calcite	Quartz + calcite ± dolomite	Oxidized minerals
Pyrite	▬		
Sphalerite	▬		
Galena	▬		
Quartz	▬	—	
Calcite	▬	—	
Dolomite	▬	—	
Smithsonite			▬
Limonite			▬
Cerusite			▬

— less, ▬ more.

between brown sphalerite and quartz (Fig. 4I), suggesting that yellow sphalerite formed later than brown sphalerite. Mineral paragenesis is shown in Table 1.

3.6. Wall rock alteration

Wall rock alteration is characterized by pyritic, siliceous, ferruginous and carbonate minerals (Wang et al., 2011). Pyritic (pyrite) alteration usually occurs in sandstone of the Shiniangluo Formation. Siliceous (quartz) alteration is weak in slate of the Shiniangluo Formation, whereas it is better developed in the Upper Cambrian dolostone (Fig. 4G). Ferruginous (limonite) and carbonates (calcite and dolomite) alterations are commonly associated with Pb–Zn mineralization in the Anle deposit area.

4. Samples and analytical methods

Representative sulfide ores and wall rocks hand specimens from drill cores and subsurface were collected. Samples were crushed, and sphalerite (brown, brownish-yellow and yellow), pyrite, galena and calcite separates were handpicked from these specimens using a binocular microscope for S, Zn and Pb, and C–O isotope analyses, respectively. In addition, dolostone, and sandstone and slate whole-rock samples were collected for C–O and Pb isotope analyses, respectively.

4.1. C–O isotope analysis

$\delta^{13}C$ and $\delta^{18}O$ values were obtained using a Finnigan MAT-253 mass spectrometer at the State Key Laboratory of Environmental Geochemistry, Chinese Academy of Sciences. Hydrothermal calcite separates and dolostone whole-rock samples were reacted with pure phosphoric acid to produce CO_2. The analytical precisions (2σ) are ±0.3‰ for $\delta^{13}C$ value and ±0.6‰ for $\delta^{18}O$ value. C–O isotopic compositions are reported relative to the Vienna Pee Dee Belemnite (V-PDB). $\delta^{18}O_{SMOW} = 1.03086 \times \delta^{18}O_{PDB} + 30.86$ (Friedman and O'Neil, 1977).

4.2. S isotope analysis

Sulfur isotope analysis was undertaken at the State Key Laboratory of Environmental Geochemistry, Chinese Academy of Sciences, by using a continuous flow isotope ratio mass spectrometer. Chinese GBW 04415 and GBW 04414 Ag_2S were used as external standards and the Vienna Canyon Diablo Troilite (V-CDT) as reference standard, with an analytical precision of ±0.3‰ (2σ) for $\delta^{34}S$ value.

4.3. Zn isotope analysis

Sphalerite grains were digested in HCl and then taken up in 6 N HCl + 0.001% H_2O_2. Zn was extracted from matrix using ion exchange chromatography (Tang et al., 2006), a modified procedure from that described by Maréchal et al. (1999). H_2O used in the experiment was purified using the Milli-Q system, with electric resistance of 18.2 MΩ. HCl was purified by sub-boiling distillation and the purification of all reagents was completed in an ultra-clean laboratory. Zinc isotope analysis was carried out using a Nu Plasma high resolution multi-collector inductively coupled plasma mass spectrometry (HR MC-ICP-MS) at Key Laboratory of Isotope Geology, Ministry of Land and Resources, Institute of Geology, Chinese Academy of Geological Sciences (Li et al., 2008; Zhou et al., 2014a, 2014b). Mass discrimination effects were corrected using a combined sample-standard bracketing and inter-element correction procedure (Li et al., 2008; Zhu et al., 2000, 2002). Accuracy and reproducibility was assessed by replicate analyses of the international standard BCR-2 (basalt), which yielded an average $\delta^{66}Zn$ value of 0.29 ± 0.04‰ (2σ, $n = 8$), within errors in agreement with previously published by Zhou et al. (2014a, 2014b). Samples AL-08-57-2 and AL-08-79-2 (brown–yellow sphalerite) were used for procedural repeats. Each result is the average value over N number of repeats, and all results are reported relative to the Lyon JMC 3-0749L Zn standard (Maréchal et al., 1999).

4.4. Pb isotope analysis

Pb isotope analysis was carried out using a GV Isoprobe-T thermal ionization mass spectrometer (TIMS) at the Beijing Institute of Uranium Geology. The analytical procedure involved dissolution of samples using HF and $HClO_4$ in crucibles, followed by basic anion exchange resin to purify Pb. Analytical results for the standard NBS 981 are $^{206}Pb/^{204}Pb = 16.935 \pm 0.003$ (2σ, $n = 8$), $^{207}Pb/^{204}Pb = 15.456 \pm 0.003$ (2σ, $n = 8$) and $^{208}Pb/^{204}Pb = 36.613 \pm 0.004$ (2σ, $n = 8$).

5. Analytical results

5.1. C–O isotopic composition

$\delta^{13}C_{PDB}$ and $\delta^{18}O_{SMOW}$ values of hydrothermal calcite and the ore-hosting dolostone whole-rock samples are listed in Table 2 and shown in Fig. 5. Calcite has $\delta^{13}C_{PDB}$ and $\delta^{18}O_{SMOW}$ values ranging from −4.8‰ to −0.2‰ (average −1.7‰, $n = 7$) and +17.9‰ to +21.4‰ (average +19.6‰, $n = 7$), respectively. $\delta^{13}C_{PDB}$ and $\delta^{18}O_{SMOW}$ values of dolostone range from +0.1‰ to +1.1‰ (average +0.6‰, $n = 3$) and +23.2‰ to +24.1‰ (average +23.6‰, $n = 3$), respectively. The Upper Cambrian ore-hosting dolostone has higher $\delta^{13}C_{PDB}$ and $\delta^{18}O_{SMOW}$ values than those of calcite associated to sulfide ores (Fig. 5).

5.2. Sulfur isotopic composition

$\delta^{34}S_{CDT}$ values of sulfides and barite are given in Table 3 and shown in Fig. 6. $\delta^{34}S_{CDT}$ values of sulfides between −1.3‰ and +17.8‰ with an average value of +6.3‰ ($n = 25$). Pyrite has $\delta^{34}S_{CDT}$ values ranging from +10.6‰ to +17.8‰ (average +13.6‰, $n = 4$). The $\delta^{34}S_{CDT}$ values of sphalerite range from −1.3‰ to +7.7‰ (average +4.7‰, $n = 12$), of which three brown sphalerite samples have $\delta^{34}S_{CDT}$ values ranging from −1.3‰ to +7.3‰ (average +3.1‰) and nine brownish-yellow sphalerite samples have $\delta^{34}S_{CDT}$ values ranging from +3.5‰ to +7.7‰ (average +5.2‰). Galena has $\delta^{34}S_{CDT}$ values ranging from +2.5‰ to +10.1‰ (average +5.1‰, $n = 9$). One barite separate from the Lower Ordovician strata has $\delta^{34}S_{CDT}$ value of +19.8‰. The $\delta^{34}S$ values of pyrite are significantly higher than those of sphalerite and galena, but sphalerite has lower $\delta^{34}S$ values lower those of galena despite some overlapping (Fig. 6B). However, in the same sample (AL-08-57; Fig. 6C), sphalerite (AL-08-57-2) has higher $\delta^{34}S$ value than galena (AL-08-57-3). In addition, the entire sulfide samples have lower $\delta^{34}S$ values than that of barite (Fig. 6A, B). In addition, the $\delta^{34}S$ values of brown sphalerite are lower than those of brownish-yellow sphalerite despite some overlapping (Table 3; Fig. 6C).

Table 2
$\delta^{13}C_{PDB}$ and $\delta^{18}O_{SMOW}$ values of calcite separate and dolostone in the Anle deposit.

No.	Mineral assemblage	Mineral/rock	$\delta^{13}C_{PDB}$/‰	$\delta^{18}O_{SMOW}$/‰	Source
AL-08-11-4	Sphalerite–galena–calcite	Calcite	−1.4	+18.8	This paper
AL-08-19-4	Sphalerite–galena–calcite	Calcite	−1.5	+18.2	
AL-08-21-4	Sphalerite–galena–calcite	Calcite	−0.6	+20.0	
AL-08-22-4	Sphalerite–galena–quartz–calcite	Calcite	−2.5	+19.8	
AL-08-79-4	Sphalerite–quartz–calcite	Calcite	−0.2	+21.4	
AL-08-80-4	Sphalerite–galena–quartz–calcite	Calcite	−0.6	+21.0	
AL-08-105-4	Sphalerite–galena–pyrite quartz–calcite	Calcite	−4.8	+17.9	
AL-08-82	Dolostone of Upper Cambrian	Dolostone	+0.1	+23.2	
AL-08-85	Dolostone of Upper Cambrian	Dolostone	+0.5	+24.1	
YCG-08-7	Dolostone of Upper Cambrian	Dolostone	+1.1	+23.6	

$\delta^{18}O_{SMOW} = 1.03086 \times \delta^{18}O_{PDB} + 30.86$ (Friedman and O'Neil, 1977).

5.3. Zinc isotopic composition

δ^{66}Zn values of sphalerite from the Anle deposit are listed in Table 4 and shown in Fig. 7. Sphalerite from the Anle deposit yields δ^{66}Zn values ranging from +0.08‰ to +0.50‰, with an arithmetic average value of +0.25‰ and a weighted average value of +0.23 ± 0.08‰ ($n = 14$). Brown, brownish-yellow and yellow sphalerite has δ^{66}Zn values ranging from +0.08‰ to +0.10‰ (average +0.09‰, $n = 3$), +0.12‰ to +0.38‰ (average +0.24‰, $n = 8$) and +0.40‰ to +0.50‰ (average +0.46‰, $n = 3$), respectively. Yellow sphalerite has higher δ^{66}Zn values than those of brown and brownish-yellow sphalerite (Fig. 7A). In the same sample (such as AL-08-5; Fig. 7B), yellow sphalerite has δ^{66}Zn value higher than that of brown sphalerite.

5.4. Lead isotopic composition

Lead isotopic compositions of sulfide minerals from the Anle Zn–Pb deposit and wall rock samples are listed in Table 5 and shown in Fig. 8. Two sandstone samples from the upper section of the Lower Ordovician Shiniangluo Formation have $^{206}Pb/^{204}Pb$ ratios of 18.539 and 18.868, $^{207}Pb/^{204}Pb$ ratios of 15.733 and 15.738, and $^{208}Pb/^{204}Pb$ ratios of 38.443 and 38.578. One slate sample from the lower section of the Lower Ordovician Shiniangluo Formation has $^{206}Pb/^{204}Pb$, $^{207}Pb/^{204}Pb$ and $^{208}Pb/^{204}Pb$ ratios of 19.582, 15.811 and 39.603, respectively. Eight Upper Cambrian dolostone samples have $^{206}Pb/^{204}Pb$ ratios ranging from 17.695 to 17.981, $^{207}Pb/^{204}Pb$ ratios ranging from 15.584 to 15.649 and $^{208}Pb/^{204}Pb$ ratios ranging from 37.674 to 38.057. $^{206}Pb/^{204}Pb$, $^{207}Pb/^{204}Pb$ and $^{208}Pb/^{204}Pb$ ratios for 12 sulfide minerals range from 17.626 to 17.856, 15.583 to 15.690 and 37.618 to 37.954, respectively, of which three galena samples have $^{206}Pb/^{204}Pb$ ratios ranging from 17.685 to 17.800, $^{207}Pb/^{204}Pb$ ratios ranging from 15.618 to 15.690 and $^{208}Pb/^{204}Pb$ ratios ranging from 37.736 to 37.954. Sandstone and slate of the Lower Ordovician Shiniangluo Formation contain more radiogenic Pb than sulfides and the Upper Cambrian ore-hosting dolostone (Fig. 8). Additionally, there is no difference of Pb isotopes among pyrite, sphalerite and galena (Table 5), suggesting that they may have had similar source for metals.

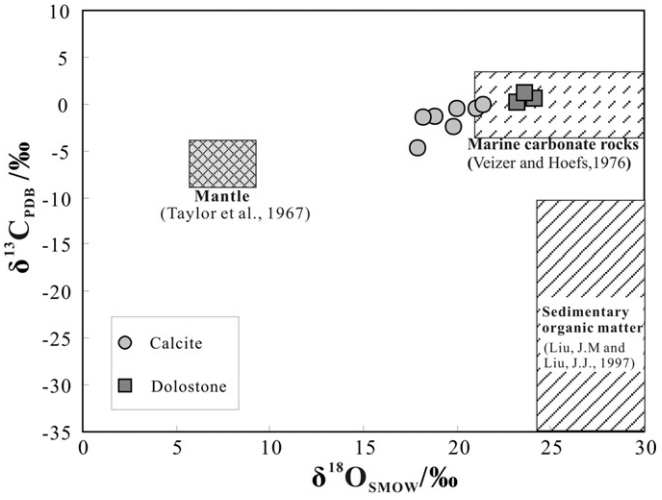

Fig. 5. Plot of $\delta^{13}C_{PDB}$ vs. $\delta^{18}O_{SMOW}$ for hydrothermal calcite and the ore-hosting dolostone from the Anle Zn–Pb deposit.

6. Discussion

6.1. Causes of zinc isotope fractionation

Significant variations of δ^{66}Zn values were reported in sphalerite from different Pb–Zn ore deposit types, such as Mississippi Valley-type (MVT), Sedimentary Exhalative (SEDEX) and volcanic massive sulfide (VMS) (Albarède, 2004; Gagnevin et al., 2012; Kelley et al., 2009; Mason et al., 2005; Pašava et al., 2014; Wilkinson et al., 2005; Zhou et al., 2014a, 2014b). Three hypotheses have been proposed to explain such variations: (i) temperature (Mason et al., 2005; Pašava et al., 2014; Toutain et al., 2008), (ii) mixing of multiple Zn sources (Wilkinson et al., 2005), and (iii) fractional crystallization (Gagnevin et al., 2012; Kelley et al., 2009; Zhou et al., 2014a, 2014b).

Previous studies have shown that at low to medium temperatures (below 250 °C), there is no correlation between δ^{66}Zn values and temperatures, either in laboratories (30–50 °C; Archer et al., 2004; Maréchal and Sheppard, 2002) or in natural hydrothermal fluids (60–250 °C; Wilkinson et al., 2005). However, at high temperatures (above 250 °C), a systematic increase in δ^{66}Zn values (−0.03‰ to +0.23‰) was observed with increasing distance from the hydrothermal vent (ca. 300 °C) in the Alexandrinka VMS deposit, Urals, Russia (Mason et al., 2005). Furthermore, a Rayleigh distillation model of temperature dependent Zn isotope fractionation ($1000\ln\alpha_{solid/vapor} = C_1 + C_2/T + C_3/T^2$, with $C_1 = 0$, $C_2 = -0.88 \times 10^3$, $C_3 = 1.00 \times 10^6$; T in degrees Kelvin) was used to explain the difference in δ^{66}Zn values between fumarolic gases (+0.05‰ to +0.85‰) and condensates (+1.48‰ to +1.68‰) in the Woro fumarolic field (590–297 °C), Merapi volcano, Indonesia (Toutain et al., 2008). Studies of fluid inclusions in quartz from the Anle deposit indicate that the homogenization temperatures are between 130 °C and 370 °C, whereas sphalerite mainly precipitated at rather low temperatures (190–270 °C; Wang et al., 2011). Therefore, we interpret that T changes was not the key factor in the observed variations of Zn isotopes (Fig. 7A). The ore-forming metals were mainly sourced from the Upper Cambrian hosting dolostone as suggested by Pb isotopes (Section 6.3), precluding the mixing of multiple Zn sources as a key control on the Zn isotope variations (Fig. 7A, B). Fractional crystallization has been used to explain the variations of δ^{66}Zn values in sphalerite from many MVT, SEDEX and VMS deposits (Gagnevin et al., 2012; Kelley et al., 2009; Mason et al., 2005; Wilkinson et al., 2005; Zhou et al., 2014a, 2014b). Previous studies have indicated that the earliest sphalerite precipitated from the hydrothermal systems is enriched in light Zn isotopes, followed by

Table 3
S isotopic compositions of sulfide and sulfate separates in the Anle deposit.

No.	Object	$\delta^{34}S_{CDT}$/‰	No.	Object	$\delta^{34}S_{CDT}$/‰	Source
AL-08-4-1	Pyrite	+17.8	AL-08-5-2	Brown sphalerite	−1.3	This paper
AL-08-5-1	Pyrite	+10.6	AL-08-22-2	Brownish-yellow sphalerite	+7.7	
AL-08-12-1	Pyrite	+10.6	AL-08-54-2	Brown sphalerite	+3.4	
AL-08-26-1	Pyrite	+15.2	AL-08-57-2	Brownish-yellow sphalerite	+3.6	
AL-08-4-3	Galena	+8.3	AL-08-79-2	Brownish-yellow sphalerite	+4.9	
AL-08-12-3	Galena	+5.7	AL-08-79-2[a]	Brownish-yellow sphalerite	+4.9	
AL-08-26-3	Galena	+10.1	AL-08-80-2	Brownish-yellow sphalerite	+3.5	
AL-08-57-3	Galena	+2.8	AL-08-80-2[a]	Brownish-yellow sphalerite	+3.6	
AL-08-83-3	Galena	+5.6	AL-08-83-2	Brownish-yellow sphalerite	+7.2	
AL-08-103-3	Galena	+4.8	AL-08-100-2	Brownish-yellow sphalerite	+5.8	
YCG-08-6-3	Galena	+3.2	AL-08-101-2	Brown sphalerite	+7.3	
YCG-08-9-3	Galena	+2.7	AL-08-103-2	Brownish-yellow sphalerite	+5.7	
YCG-08-18-3	Galena	+2.5	Br-1	Barite in Lower Ordovician strata	+19.8	

[a] Samples are used for procedural repeats.

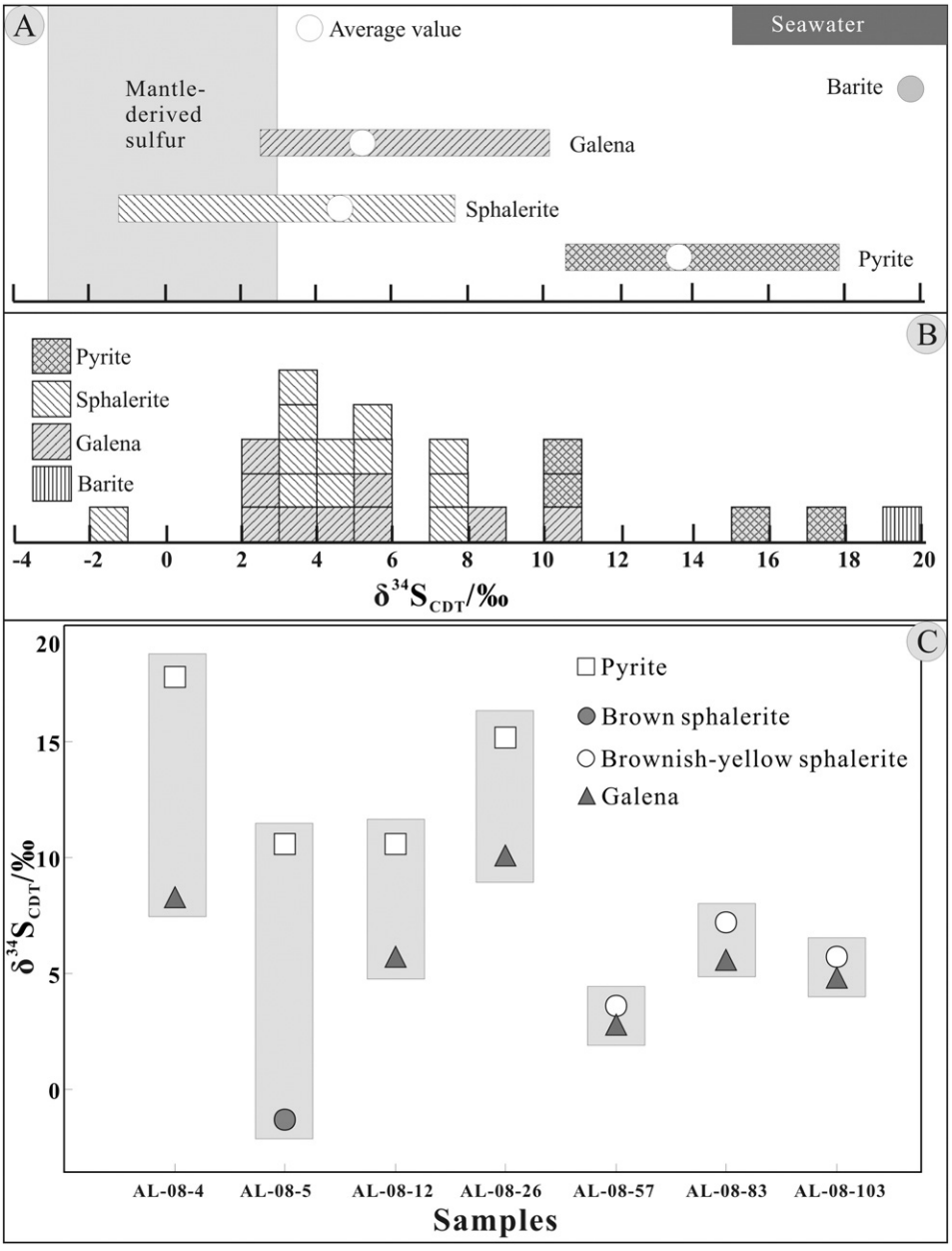

Fig. 6. A: the $\delta^{34}S_{CDT}$ values of the Anle Zn–Pb deposit compared with those of mantle, seawater and evaporites; B: sulfur isotopic composition histogram of the Anle deposit; C: the $\delta^{34}S_{CDT}$ values for symbiotic sulfide mineral pairs.

Table 4
Zn isotopic compositions of sphalerite separates from the Anle deposit.

No.	Object	$\delta^{66}Zn_{JMC}$/‰[a]	SD	NA	Source
AL-08-5-2	Brown sphalerite	+0.09	0.02	0.02	This paper
AL-08-5-5	Yellow sphalerite	+0.40	0.03	0.03	
AL-08-22-2	Brownish-yellow sphalerite	+0.12	0.02	0.02	
AL-08-22-5	Yellow sphalerite	+0.50	0.03	0.03	
AL-08-54-2	Brown sphalerite	+0.08	0.02	0.02	
AL-08-54-5	Brownish-yellow sphalerite	+0.24	0.02	0.02	
AL-08-57-2	Brownish-yellow sphalerite	+0.28	0.02	0.02	
AL-08-57-2[b]	Brownish-yellow sphalerite	+0.25	0.03	0.03	
AL-08-79-2	Brownish-yellow sphalerite	+0.37	0.02	0.02	
AL-08-79-2[b]	Brownish-yellow sphalerite	+0.38	0.02	0.02	
AL-08-100-2	Brownish-yellow sphalerite	+0.14	0.02	0.02	
AL-08-100-5	Yellow sphalerite	+0.49	0.03	0.03	
AL-08-101-2	Brown sphalerite	+0.10	0.02	0.02	
AL-08-103-2	Brownish-yellow sphalerite	+0.12	0.03	0.03	

SD, standard deviation; NA, number of analyses.
[a] Mean over n number of repeats.
[b] Samples are used for procedural repeats.

progressively heavier ones (Archer et al., 2004; Maréchal and Sheppard, 2002). Since brown sphalerite preceded yellow sphalerite in the Anle deposit (Fig. 4I), we interpret the lighter to heavier Zn isotopes trend (Fig. 7A, B) as a result of kinetic (Rayleigh-type) fractionation.

Additionally, similar to sphalerite from the Cévennes ($\delta^{66}Zn = -0.06‰$ to $+0.42‰$; Albarède, 2004; relative to JMC Zn standard, same below), Picos de Europa ($\delta^{66}Zn = -0.82‰$ to $+0.07‰$) and La Florida ($\delta^{66}Zn = -0.87‰$ to $-0.08‰$; Pašava et al., 2014), Midlands ($\delta^{66}Zn = -0.17‰$ to $+0.64‰$, with one value at $+1.33‰$; Wilkinson et al., 2005) and Navan ($\delta^{66}Zn = -0.32‰$ to $+0.23‰$; Gagnevin et al., 2012) MVT Pb–Zn deposits in Europe, the SYG-type (different from typical MVT) deposits in western Yangtze Block, southwest China ($\delta^{66}Zn = -0.24‰$ to $+0.71‰$; Zhou et al., 2014a, 2014b), the Red Dog SEDEX deposit in the USA ($\delta^{66}Zn = 0.00‰$ to $+0.60‰$; Kelley et al., 2009), and the Alexandrinka VMS deposit in Russia ($\delta^{66}Zn = -0.43‰$ to $+0.23‰$; Mason et al., 2005), sphalerite from the Anle Zn–Pb deposit shows a variation of Zn isotopic composition (Fig. 9). This suggests that Zn isotopes are not the best tools for discriminating ore deposit types.

6.2. Source of ore-forming fluids

In general, hydrothermal fluids obtain carbon from three main reservoirs: (i) mantle, (ii) marine carbonate rocks, and (iii) sedimentary organic matter (e.g., Demény and Harangi, 1996; Demény et al., 1998; Liu and Liu, 1997; Taylor et al., 1967; Veizer and Hoefs, 1976). The $\delta^{13}C_{PDB}$ and $\delta^{18}O_{SMOW}$ values for mantle, marine carbonate and organic matter range from $-4.0‰$ to $-8.0‰$ and $+6.0‰$ to $+10.0‰$ (Taylor et al., 1967), $-4.0‰$ to $+4.0‰$ and $+20.0‰$ to $+30.0‰$ (Veizer and

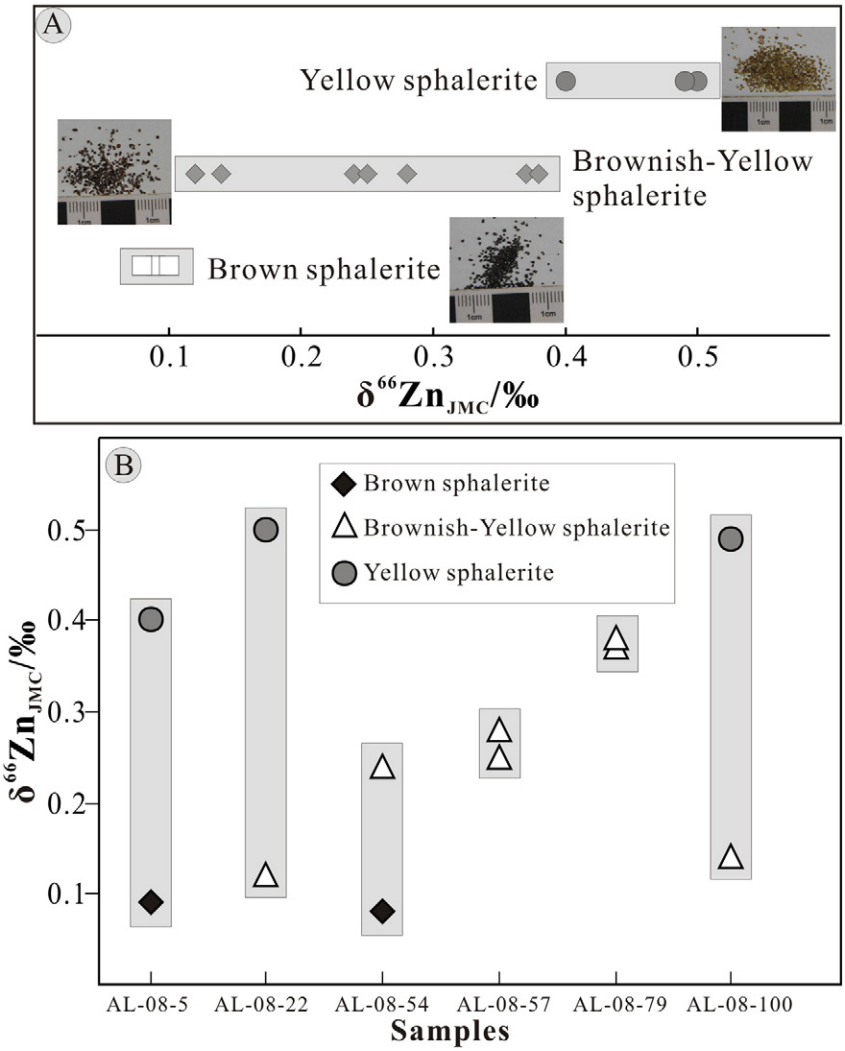

Fig. 7. A: $\delta^{66}Zn_{JMC}$ values of different color sphalerite from the Anle Zn–Pb deposit; B: variations of Zn isotopes in different color sphalerite from the same hand specimens.

Table 5
Pb isotopic compositions of sulfide separates and wall rocks in the Anle deposit.

No.	Rock/mineral	Source	$^{206}Pb/^{204}Pb$[b]	$^{207}Pb/^{204}Pb$[b]	$^{208}Pb/^{204}Pb$[b]	Source
AL-08-58	Sandstone	O_1 Shinianluo Fm., upper section	18.868	15.733	38.578	This paper
YCG-08-14	Sandstone	O_1 Shinianluo Fm., upper section	18.539	15.738	38.443	
AL-08-76	Slate	O_1 Shinianluo Fm., lower section	19.582	15.811	39.603	
AL-08-82	Dolostone	Upper Cambrian	17.695	15.597	37.674	
AL-08-85	Dolostone	Upper Cambrian	17.715	15.603	37.677	
YCG-08-7	Dolostone	Upper Cambrian	17.981	15.649	38.057	
AL-08-15	Dolostone	Upper Cambrian	17.896	15.627	37.818	
AL-08-28	Dolostone	Upper Cambrian	17.739	15.605	37.710	
AL-08-74	Dolostone	Upper Cambrian	17.776	15.584	37.694	
AL-08-86	Dolostone	Upper Cambrian	17.775	15.604	37.777	
YCG-08-1	Dolostone	Upper Cambrian	17.733	15.616	37.727	
YCG-08-4-3	Galena	Sphalerite–galena–pyrite ore	17.685	15.618	37.736	
AL-08-83-3	Galena	Sphalerite–galena ore	17.755	15.641	37.843	
AL-08-103-3	Galena	Sphalerite–galena ore	17.800	15.690	37.954	
AL-08-79-2	Brownish-yellow sphalerite	Sphalerite–quartz–calcite ore	17.750	15.607	37.706	
AL-08-80-2	Brownish-yellow sphalerite	Sphalerite–galena–quartz–calcite ore	17.790	15.602	37.801	
AL-08-83-5	Brown sphalerite	Sphalerite–galena ore	17.758	15.614	37.733	
AL-08-103-5	Brown sphalerite	Sphalerite–galena ore	17.752	15.617	37.738	
AL-08-79-2[a]	Brownish-yellow sphalerite	Sphalerite–quartz–calcite ore	17.728	15.587	37.708	
AL-08-80-5	Yellow sphalerite	Sphalerite–galena–quartz–calcite ore	17.856	15.611	37.885	
AL-08-4-1	Pyrite	Sphalerite–galena–pyrite–quartz ore	17.678	15.607	37.709	
AL-08-5-1	Pyrite	Pyrite–sphalerite ore	17.697	15.603	37.720	
AL-08-26-1	Pyrite	Pyrite–galena ore	17.626	15.583	37.618	

O_1 = Lower Ordovician.
[a] Sample is used for procedural repeat.
[b] Pb isotopic data for the wall rock samples are age-corrected at ca. 210 Ma.

Hoefs, 1976), and −30.0‰ to −10.0‰ and +24.0‰ to +30.0‰ (Liu and Liu, 1997), respectively (Fig.5). Calcite from the Anle deposit has higher $\delta^{13}C_{PDB}$ and $\delta^{18}O_{SMOW}$ values than mantle and sedimentary organic matter, but similar to marine carbonate rocks and the ore-hosting dolostone (Fig. 5). This indicates that mantle and organic matter may not have contributed significant carbon to the hydrothermal fluids. The similarity of $\delta^{13}C_{PDB}$ and $\delta^{18}O_{SMOW}$ values between hydrothermal calcite and the Upper Cambrian ore-hosting dolostone suggests that C- and O- isotopes in hydrothermal fluids were in close thermal equilibrium with the dolostone (Gray et al., 1991; Muchez et al., 1995). Therefore, the carbon in the ore-forming fluids was likely to be provided by the ore-hosting dolostone as suggested by fluid inclusion studies (Wang et al., 2011), similar to many carbonate-hosted Pb–Zn deposits worldwide (including the SYG-type Pb–Zn deposits in western Yangtze Block, SW China; Zhou et al., 2013a, 2014b, 2015).

Ore minerals in the Anle Zn–Pb deposit include sphalerite, pyrite and galena, and gangue minerals include quartz, calcite and dolomite, whereas sulfate is absent. Previous studies demonstrate that under low oxygen conditions, $\delta^{34}S_{sulfides}$ values (especially pyrite) represent approximately the $\delta^{34}S_{fluids}$ values (e.g., Basuki et al., 2008; Dixon and Davidson, 1996; Ohmoto, 1972; Ohmoto et al., 1990; Pass et al., 2014; Seal, 2006; Zhou et al., 2013f). Pyrite from the Anle deposit has $\delta^{34}S_{CDT}$ values between +10.6‰ and +17.8‰ ($n = 4$), which are significantly higher than those of mantle-derived sulfur (0 ± 3‰; Chaussidon et al., 1989). Barite from the Lower Ordovician Shiniangluo Formation has $\delta^{34}S_{CDT}$ value of +19.8‰ (Table 3), similar to Cambrian–Triassic seawater sulfate (+15‰ to +35‰; Claypool et al., 1980; Seal, 2006), and slightly higher than those of pyrite. It is worth noting that, some sphalerite and galena analyses have yielded low $\delta^{34}S_{CDT}$ values (between −1.3‰ and +3.6‰, $n = 9$), similar to the mantle-derived sulfur. However, there is little geological evidence for magmatic activities in the Anle deposit. Therefore, we interpret that the reduced sulfur in the ore-forming fluids at Anle may have been derived from seawater sulfate. In addition, sulfates are absent in the Anle deposit, and the equilibrium–disequilibrium constraints of sulfide mineral pairs (e.g. pyrite–galena) that were deposited contemporaneously can be used as geothermometers (e.g., Czamanske and Rye, 1974; Ohmoto et al., 1990). The relations of $\delta^{34}S_{py} > \delta^{34}S_{sph}$ and $\delta^{34}S_{sph} > \delta^{34}S_{gal}$ in the

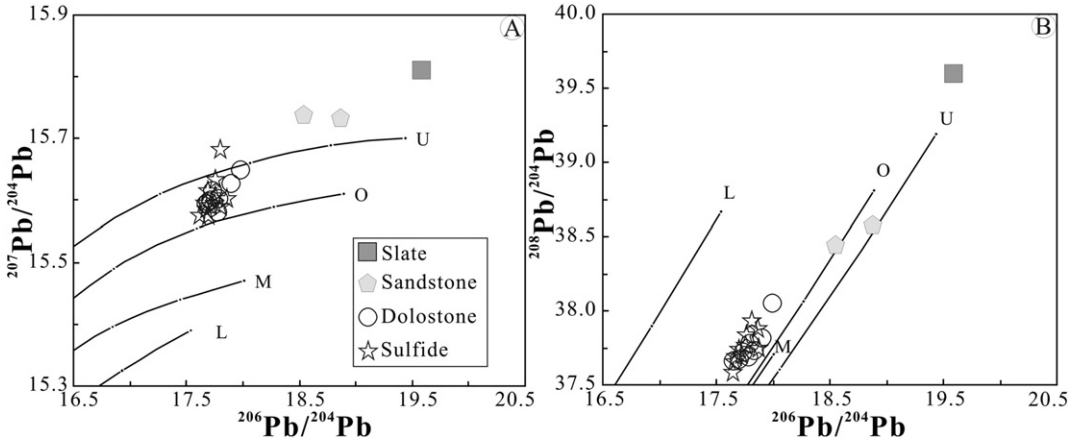

Fig. 8. Plots of $^{207}Pb/^{204}Pb$ vs. $^{206}Pb/^{204}Pb$ (A) and $^{208Pb}/^{204}Pb$ vs. $^{206}Pb/^{204}Pb$ (B) for sulfides and wall rocks in the Anle Zn–Pb deposit. Trends for the upper crust (U), orogenic belt (O), mantle (M) and lower crust (L) are from Zartman and Doe (1981).

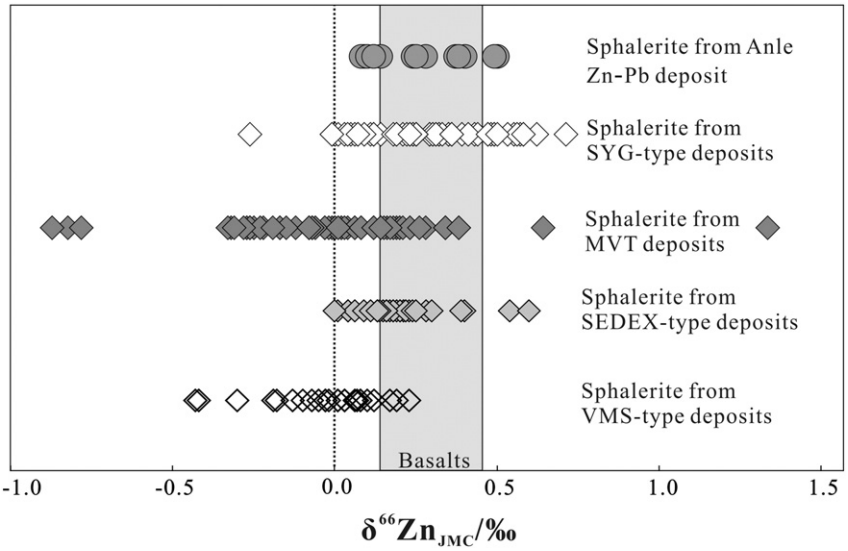

Fig. 9. Comparison of $\delta^{66}Zn_{JMC}$ values between sphalerite separates from the Anle Zn–Pb deposit, and Pb–Zn deposits of MVT, SEDEX, VMS and SYG-types. Zinc isotopic data for MVT are from Albarède (2004); Wilkinson et al. (2005); Gagnevin et al. (2012) and Pašava et al. (2014), SEDEX-type are from Kelley et al. (2009), VMS-type are from Mason et al. (2005) and SYG-type are from Zhou et al. (2014a, 2014b).

same samples suggest that sulfides may have precipitated under sulfur isotope equilibrium. The $\Delta^{34}S$ values between two pyrite–galena pairs (samples AL-08-12 and AL-08-26) from the Anle deposit indicate temperatures ($\Delta^{34}S = \delta^{34}S_{py} - \delta^{34}S_{gal} = 1.15 \times 10^6 / (T + 273.15)^2$; Czamanske and Rye, 1974) of 201 °C to 211 °C, close to the peak homogenization temperatures of fluid inclusions in quartz (190 °C to 270 °C; Wang et al., 2011). Additionally, galena and brownish-yellow sphalerite samples have higher $\delta^{34}S_{CDT}$ values than sphalerite and brown sphalerite, respectively, suggesting that disequilibrium conditions were also widespread. To sum up, we exclude bacterial sulfate reduction (BSR) to be a significant fractionation factor, since it would result in a larger sulfur isotope fractionation. Thermo-chemical reduction of sulfate to sulfide (TSR) can lower $\delta^{34}S$ values to up to +20‰ (e.g., Basuki et al., 2008; Ohmoto et al., 1990; Ohmoto and Goldhaber, 1997; Pass et al., 2014), such that the reduced sulfur in sulfide ores is interpreted to be the products of barite in the Shiniangluo Formation sedimentary rocks by TSR.

6.3. Origin of ore-forming elements

Because some Pb isotopes are radiogenic, the Pb isotopic ratios need to be corrected to a consistent age in order to make comparisons between different metallogenic phases. Sulfides have very low U and Th contents, hence radiogenic Pb is negligible and no age correction is needed, whereas age correction for the whole-rock Pb isotopes are needed (e.g., Carr et al., 1995; Muchez et al., 2005; Pass et al., 2014). The Songpan–Ganzi fold belt was formed in the Late Triassic (205–230 Ma) (e.g., Chang, 2000; Xu et al., 1992), and the formation of the Anle deposit was likely to be associated with the Songpan–Ganzi orogenic event (Wang et al., 2011). Therefore, the age 210 Ma is used for correcting the whole-rock Pb isotopes. In the $^{207}Pb/^{204}Pb$ vs. $^{206}Pb/^{204}Pb$ diagram (Fig. 8A), age-corrected sandstone and slate samples from the Lower Ordovician Shiniangluo Formation are plotted above the upper crust average Pb evolution curve (Zartman and Doe, 1981), suggesting that they may have been sourced from the crust, in agreement with their sedimentary setting. The Upper Cambrian dolostone falls between the upper crust and orogenic belt average Pb evolution curves (Zartman and Doe, 1981), indicating that the Songpan–Ganzi orogenic event may have affected the Upper Cambrian dolostone. Sulfides (except sample AL-08-80-5 yellow sphalerite) also plot between orogenic belt and upper crustal average curves (Zartman and Doe, 1981), overlapping the age-corrected ore-hosting dolostone. These data suggest that the ore Pb in the Anle Zn–Pb deposit may have been derived from the Upper Cambrian ore-hosting dolostone and affected by the Songpan–Ganzi orogenic event.

6.4. Ore genesis

Ore deposits in southwestern China may have been affected by thermo-tectonic reworking and recrystallization by multiple orogenic episodes (e.g., Zaw et al., 2007; Hu and Zhou, 2012). The Anle Zn–Pb deposit is hosted by Upper Cambrian dolostone, which means a significant difference with the setting of typical Chinese VMS deposits. Ore bodies in the Anle deposit occur as lenses that show vein, banded and brecciated structures. This indicates that the Anle deposit may have been deposited significantly later than the ore-hosting rocks and thus are epigenetic. C–O and Pb isotopes suggest that the ore-forming fluids and metals may have been sourced from the Upper Cambrian dolostone, which was affected by the Songpan–Ganzi orogenic event, and S isotopes indicate that sulfur may have been derived from evaporites by TSR. From all the above discussions, the Anle deposit is similar to typical MVT deposits (e.g., Leach et al., 2001, 2005, 2010; Muchez et al., 2005; Oliver, 1986, 1992; Pirajno, 2009, 2013). Besides, Wang et al. (2011) reported that the ore-forming fluids have medium–high temperature (130 °C to 370 °C) and low salinity (3.0–12.8 wt.% eq. NaCl), and considered that the formation of the Anle carbonate-hosted Zn–Pb deposit was a response to the Songpan–Ganzi orogenic event. Therefore, we propose that the Anle Zn–Pb deposit should be classified as an epigenetic Mississippi Valley-type deposit.

7. Conclusions

The Anle Zn–Pb deposit is hosted by Upper Cambrian dolostone in the Sanjiang tectonic belt, southwest China, and occurs within the NW-trending Anle anticline. At Anle, sulfur may have been derived from evaporites, while carbon and metals may have been sourced from the ore-hosting dolostone that was affected by the Songpan–Ganzi orogenic event. Probably due to fractional crystallization, the late yellow sphalerite has higher $\delta^{66}Zn$ than the early brown sphalerite. At Anle, Zn isotopes can't be used as useful tracers for ore-forming metals and discriminators for metallogenic setting. The Anle Zn–Pb deposit can be assigned to be an epigenetic MVT deposit.

Acknowledgments

This research was financially supported by the 12th Five-Year Plan Project of the State Key Laboratory of Ore deposit Geochemistry, Chinese Academy of Sciences (No. SKLODG-ZY125-02), the National Basic Research Program of China (No. 2014CB440905) and the National Natural Science Foundation of China (Nos. 41163001 and 41402072). Thanks are given to Prof. Xiang-Kun Zhu, Prof. Mei-Fu Zhou and Prof. Philippe Muchez for useful discussions. Comments and suggestions from Prof. Franco Pirajno (Editor-in-Chief) and two anonymous reviewers have greatly enhanced the paper.

References

Albarède, F., 2004. The stable isotope geochemistry of copper and zinc. Rev. Mineral. Geochem. 55, 409–427.
Archer, C., Vance, D., Butler, I., 2004. Abiotic Zn isotope fractionations associated with ZnS precipitation. Geochim. Cosmochim. Acta 68, A325.
Basuki, N.I., Taylor, B.E., Spooner, E.T.C., 2008. Sulfur isotope evidence for thermo-chemical reduction of dissolved sulfate in Mississippi Valley type zinc–lead mineralization, Bongara area, northern Peru. Econ. Geol. 103, 183–799.
Carr, G.R., Dean, J.A., Suppel, D.W., Heithersay, P.S., 1995. Precise lead isotope fingerprinting of hydrothermal activity associated with Ordovician to Carboniferous metallogenic events in the Lachlan fold belt of New South Wales. Econ. Geol. 90, 1467–1505.
Chang, E.Z., 2000. Geology and tectonics of the Songpan–Ganzi fold belt, southwestern China. Int. Geol. Rev. 42, 813–831.
Chaussidon, M., Albarède, F., Sheppard, S.M.F., 1989. Sulphur isotope variations in the mantle from ion microprobe analyses of micro-sulphide inclusions. Earth Planet. Sci. Lett. 92, 144–156.
Chen, J.B., Gaillardet, J., Dessert, C., Villemant, B., Louvat, P., Crispi, O., Birck, J.L., Wang, Y.N., 2013. Zn isotope compositions of the thermal spring waters of La Soufrière volcano, Guadeloupe Island. Geochim. Cosmochim. Acta 127, 67–82.
Claypool, G.E., Holser, W.T., Kaplan, I.R., Sakai, H., Zak, I., 1980. The age curves of sulfur and oxygen isotopes in marine sulfate and their mutual interpretation. Chem. Geol. 28, 199–260.
Czamanske, G.K., Rye, R.O., 1974. Experimentally determined sulfur isotope fractionations between sphalerite and galena in the temperature range 600 °C to 275 °C. Econ. Geol. 69, 17–25.
Demény, A., Ahijado, A., Casillas, R., Vennemann, T.W., 1998. Crustal contamination and fluid/rock interaction in the carbonatites of Fuerteventura (Canary Islands, Spain): a C, O, H isotope study. Lithos 44, 101–115.
Demény, A., Harangi, S.Z., 1996. Stable isotope studies on carbonate formations in alkaline basalt and lamprophyre series: evolution of magmatic fluids and magma–sediment interactions. Lithos 37, 335–349.
Dixon, G., Davidson, G.J., 1996. Stable isotope evidence for thermo chemical sulfate reduction in the Dugald River (Australia) strata-bound shale-hosted zinc-lead deposit. Chem. Geol. 129, 227–246.
Friedman, I., O'Neil, J.R., 1977. Compilation of stable isotope fractionation factors of geochemical interest. Data of Geochemistry. U.S. Geol. Surv. Prof. Pap. 1–12 (440–KK).
Fujii, T., Moynier, F., Pons, M.L., Albarède, F., 2011. The origin of Zn isotope fractionation in sulfides. Geochim. Cosmochim. Acta 75, 7632–7643.
Gagnevin, D., Boyce, A.J., Barrie, C.D., Menuge, J.F., Blakeman, R.J., 2012. Zn, Fe and S isotope fractionation in a large hydrothermal system. Geochim. Cosmochim. Acta 88, 183–198.
Gray, D.R., Gregory, R.T., Durney, D.W., 1991. Rock-buffered fluid-rock interaction in deformed quartz-rich turbidite sequences, eastern Australia. J. Geophys. Res. Solid Earth (1978–2012) 96 (B12), 19681–19704.
Gromek, P., Gleeson, S.A., Simonetti, A., 2012. A basement-interacted fluid in the N81 deposit, Pine Point Pb–Zn district, Canada: Sr isotopic analyses of single dolomite crystals. Mineral. Deposita 47, 749–754.
Han, R.S., Liu, C.Q., Huang, Z.L., Chen, J., Ma, D.Y., Lei, L., Ma, G.S., 2007. Geological features and origin of the Huize carbonate-hosted Zn–Pb–(Ag) district, Yunnan, South China. Ore Geol. Rev. 31, 360–383.
Hou, Z.Q., Cook, N.J., 2009. Metallogenesis of the Tibetan collisional orogen: a review and introduction to the special issue. Ore Geol. Rev. 36, 2–24.
Hou, Z.Q., Zaw, K., Pan, G.T., Mo, X.X., Xu, Q., Hu, Y.Z., Li, X.Z., 2007. The Sanjiang Tethyan metallogenesis in S.W. China: tectonic setting, metallogenic epoch and deposit type. Ore Geol. Rev. 31, 48–87.
Hu, R.Z., Zhou, M.F., 2012. Multiple Mesozoic mineralization events in South China—an introduction to the thematic issue. Mineral. Deposita 47, 579–588.
Huang, Z.L., Li, W.B., Chen, J., Han, R.S., Liu, C.Q., Xu, C., Guan, T., 2003. Carbon and oxygen isotope constraints on the mantle fluids join the mineralization of the Huize super large Pb–Zn deposits, Yunnan Province, China. J. Geochem. Explor. 78/79, 637–642.
Huang, Z.L., Li, X.B., Zhou, M.F., Li, W.B., Jin, Z.G., 2010. REE and C–O isotopic geochemistry of calcites from the world class Huize Pb–Zn deposit, Yunnan, China: implications for the ore genesis. Acta Geol. Sin. 84, 597–613 (Eng. Ed.).
John, S.G., Rouxel, O.J., Craddock, P.R., Engwall, A.M., Boyle, E.A., 2008. Zinc stable isotopes in seafloor hydrothermal vent fluids and chimneys. Earth Planet. Sci. Lett. 269, 17–28.
Kelley, K.D., Wilkinson, J.J., Chapman, J.B., Crowther, H.L., Weiss, D.J., 2009. Zinc isotopes in sphalerite from base metal deposits on the Red Dog district, Northern Alaska. Econ. Geol. 104, 767–773.
Leach, D.L., Bradley, D., Lewchuk, M.T., Symons, D.T.A., de Marsily, G., Brannon, J., 2001. Mississippi Valley type lead–zinc deposits through geological time: implications from recent age-dating research. Mineral. Deposita 36, 711–740.
Leach, D.L., Sangster, D., Kelley, K., Large, R.R., Garven, G., Allen, C., Gutzmer, J., Walters, S.G., 2005. Sediment-hosted lead–zinc deposits: a global perspective. Econ. Geol. 561–608 (100th Anniversary volume).
Leach, D.L., Bradley, D.C., Huston, D., Pisarevsky, S.A., Taylor, R.D., Gardoll, S.J., 2010. Sediment-hosted lead–zinc deposits in Earth history. Econ. Geol. 105, 593–625.
Li, B., Zhou, J.X., Huang, Z.L., Yan, Z.F., Bao, G.P., Sun, H.R., 2015. Geological, rare earth elemental and isotopic constraints on the origin of the Banbanqiao Zn–Pb deposit, southwest China. J. Asian Earth Sci. 111, 100–112.
Li, S.Z., Zhu, X.K., Tang, S.H., He, X.X., Cai, J.J., 2008. The application of MC-ICP-MS to high-precision measurement of Zn isotope ratios. Acta Petrol. Mineral. 27, 273–278 (in Chinese with English abstract).
Liu, H.C., Lin, W.D., 1999. Study on the Law of Pb–Zn–Ag Ore Deposit in Northeast Yunnan. China. Yunnan University Press, Kunming, pp. 1–468 (in Chinese).
Liu, J.M., Liu, J.J., 1997. Basin fluid genetic model of sediment-hosted micro-disseminated gold deposits in the gold-triangle area between Guizhou, Guangxi and Yunnan. Acta Mineral. Sin. 17, 448–456 (in Chinese with English abstract).
Maréchal, C.N., Sheppard, S.M.F., 2002. Isotopic fractionation of Cu and Zn between chloride and nitrate solutions and malachite or smithsonite at 30 °C and 50 °C. Goldschmidt Conference. Geochim. Cosmochim. Acta 66, A484.
Maréchal, C.N., Télouk, P., Albarède, F., 1999. Precise analysis of copper and zinc isotopic compositions by plasma-source mass spectrometry. Chem. Geol. 156, 251–273.
Mason, T.F.D., Weiss, D.J., Chapman, J.B., Wilkinson, J.J., Tessalina, S.G., Spiro, B., Horstwood, M.S.A., Spratt, J., Coles, B.J., 2005. Zn and Cu isotopic variability in the Alexandrinka volcanic-hosted massive sulphide (VHMS) ore deposit, Urals, Russia. Chem. Geol. 221, 170–187.
Mirnejad, H., Simonetti, A., Molasalehi, F., 2011. Pb isotopic compositions of some Zn–Pb deposits and occurrences from Urumieh–Dokhtar and Sanandaj–Sirjan Zones in Iran. Ore Geol. Rev. 39, 181–187.
Muchez, P., Heijlen, W., Banks, D., Blundell, D., Boni, M., Grandia, F., 2005. Extensional tectonics and the timing and formation of basin-hosted deposits in Europe. Ore Geol. Rev. 27, 241–267.
Muchez, P., Slobodník, M., Viaene, W.A., Keppens, E., 1995. Geochemical constraints on the origin and migration of palaeofluids at the northern margin of the Variscan foreland, southern Belgium. Sediment. Geol. 96, 191–200.
Ohmoto, H., Goldhaber, M.B., 1997. Sulfur and carbon isotopes. In: Barnes, H.L. (Ed.), Geochemistry of Hydrothermal Ore Deposits, 3rd ed. Wiley and Sons, New York, pp. 517–611.
Ohmoto, H., Kaiser, C.J., Geer, K.A., Ho, S.E., 1990. Systematics of sulphur isotopes in recent marine sediments and ancient sediment-hosted base metal deposits. In: Herbert, H.K. (Ed.), Stable Isotopes and Fluid Processes in Mineralization. Geol. Dep. Univ. Extens. Univ. Western Australia 23, pp. 70–120.
Ohmoto, H., 1972. Systematics of sulfur and carbon isotopes in hydrothermal ore deposits. Econ. Geol. 67, 551–579.
Oliver, J., 1986. Fluids expelled tectonically from orogenic belts: their role in hydrocarbon migration and other geologic phenomena. Geology 14, 99–102.
Oliver, J., 1992. The spots and stains of plate tectonics. Earth Sci. Rev. 32, 77–106.
Palinkaš, S.S., Palinkaš, L.A., Renac, C., Spangenberg, J.E., Lüders, V., Molnar, F., Maliqi, G., 2013. Metallogenic model of the Trepča Pb–Zn–Ag skarn deposit, Kosovo: evidence from fluid inclusions, rare earth elements, and stable isotope data. Econ. Geol. 108, 135–162.
Pašava, J., Tornos, F., Chrastný, V., 2014. Zinc and sulfur isotope variation in sphalerite from carbonate-hosted zinc deposits, Cantabria, Spain. Mineral. Deposita 49, 797–807.
Pass, H.E., Cooke, D.R., Davidson, G., Maas, R., Dipple, G., Rees, C., Ferreira, L., Taylor, C., Deyell, C.L., 2014. Isotope geochemistry of the northeast zone, Mount Polley Alkalic Cu–Au–Ag porphyry deposit, British Columbia: a case for carbonate assimilation. Econ. Geol. 109, 859–890.
Pirajno, F., 2009. Hydrothermal Processes and Mineral Systems. Springer, Berlin, p. 1256.
Pirajno, F., 2013. The Geology and Tectonic Setting of China's Mineral Deposits. Springer, Berlin, pp. 123–183.
Seal, I.R., 2006. Sulfur isotope geochemistry of sulfide minerals. Rev. Mineral. Geochem. 61, 633–677.
Tang, S.H., Zhu, X.K., Cai, J.J., Li, S.Z., He, X.X., Wang, J.H., 2006. Chromatographic separation of Cu, Fe and Zn using AG MP-1 anion exchange resin for isotope determination by MC-ICPMS. Rock Miner. Analy. 25, 5–8 (in Chinese with English abstract).
Tang, Y.Y., Bi, X.W., Fayek, M.F., Hu, R.Z., Wu, L.Y., Zou, Z.C., Feng, C.X., Wang, X.S., 2014. Microscale sulfur isotopic compositions of sulfide minerals from the Jinding Zn–Pb deposit, Yunnan Province, Southwest China. Gondwana Res. 26, 594–607.
Taylor, J.H.P., Frechen, J., Degens, E.T., 1967. Oxygen and carbon isotope studies of carbonatites from the Laacher See District, West Germany and the Alno District Sweden. Geochim. Cosmochim. Acta 31, 407–430.
Toutain, J.P., Sonke, J., Munoz, M., Nonell, A., Polvé, M., Viers, J., Freydier, R., Sortino, F., Joron, J.L., Sumarti, S., 2008. Evidence for Zn isotopic fractionation at Merapi volcano. Chem. Geol. 253, 74–82.
Veizer, J., Hoefs, J., 1976. The nature of $^{18}O/^{16}O$ and $^{13}C/^{12}C$ secular trends in sedimentary carbonate rocks. Geochim. Cosmochim. Acta 40, 1387–1395.
Wang, C., Deng, J., Carranza, E.J.M., Lai, X., 2014. Nature, diversity and temporal–spatial distribution of sediment-hosted Pb–Zn deposits in China. Ore Geol. Rev. 56, 327–351.
Wang, F., Huang, Z.L., Li, B., Ding, W., Zhu, M.B., 2011. Fluid inclusions of the Anle Pb–Zn deposit in the northwestern Yunnan province, China. Acta Miner. Sin. 31, 441–448 (in Chinese with English abstract).
Wilkinson, J.J., Weiss, D.J., Mason, T.F.D., Coles, B.J., 2005. Zinc isotope variation in hydrothermal systems: preliminary evidence from the Irish Midlands ore field. Econ. Geol. 100, 583–590.

Xu, Z.Q., Hou, L.W., Wang, Z.X., 1992. Orogenic Processes of the Songpan–Ganzi Orogenic Belt of China. Geol. Publ. House, Beijing, pp. 1–190 (In Chinese).
Xue, C.J., Zeng, R., Liu, S.W., Chi, G.X., Qing, H.R., Chen, Y.C., Yang, J.D., Wang, D.H., 2007. Geologic, fluid inclusion and isotopic characteristics of the Jinding Zn–Pb deposit, western Yunnan, South China: a review. Ore Geol. Rev. 31, 337–359.
Ye, L., Cook, N.J., Ciobanu, C.L., Liu, Y.P., Zhang, Q., Liu, T.G., Gao, W., Yang, Y.L., Danyushevsky, L., 2011. Trace and minor elements in sphalerite from base metal deposits in South China: a LA-ICPMS study. Ore Geol. Rev. 39, 188–217.
Zartman, R.E., Doe, B.R., 1981. Plumbotectonics—the model. Tectonophysics 75, 135–162.
Zaw, K., Peters, S.G., Cromie, P., Burrett, C., Hou, Z., 2007. Nature, diversity of deposit types and metallogenic relations of South China. Ore Geol. Rev. 31, 3–47.
Zhang, J.R., Wen, H.J., Qiu, Y.Z., Zhang, Y.X., Li, C., 2013. Ages of sediment-hosted Himalayan Pb–Zn–Cu–Ag polymetallic deposits in the Lanping basin, China: Re–Os geochronology of molybdenite and Sm–Nd dating of calcite. J. Asian Earth Sci. 73, 284–295.
Zheng, M.H., Wang, X.C., 1991. Genesis of the Daliangzi Pb–Zn deposit in Sichuan, China. Econ. Geol. 86, 831–846.
Zhou, C.X., Wei, C.S., Guo, J.Y., 2001. The source of metals in the Qilingchang Pb–Zn deposit, Northeastern Yunnan, China: Pb–Sr isotope constraints. Econ. Geol. 96, 583–598.
Zhou, J.X., Huang, Z.L., Zhou, M.F., Li, X.B., Jin, Z.G., 2013a. Constraints of C–O–S–Pb isotope compositions and Rb–Sr isotopic age on the origin of the Tianqiao carbonate-hosted Pb–Zn deposit, SW China. Ore Geol. Rev. 53, 77–92.
Zhou, J.X., Gao, J.G., Chen, D., Liu, X.K., 2013b. Ore genesis of the Tianbaoshan carbonate-hosted Pb–Zn deposit, Southwest China: geologic and isotopic (C–H–O–S–Pb) evidence. Int. Geol. Rev. 55, 1300–1310.
Zhou, J.X., Huang, Z.L., Bao, G.P., 2013c. Geological and sulfur–lead–strontium isotopic studies of the Shaojiwan Pb–Zn deposit, southwest China: implications for the origin of hydrothermal fluids. J. Geochem. Explor. 128, 51–61.
Zhou, J.X., Huang, Z.L., Yan, Z.F., 2013d. The origin of the Maozu carbonate-hosted Pb–Zn deposit, southwest China: constrained by C–O–S–Pb isotopic compositions and Sm–Nd isotopic age. J. Asian Earth Sci. 73, 39–47.
Zhou, J.X., Wang, J.S., Yang, D.Z., Liu, J.H., 2013e. H–O–S–Cu–Pb isotopic constraints on the origin of the Nage Cu–Pb deposit, southeast Guizhou Province, SW China. Acta Geol. Sin. 87, 1334–1343 (Eng. Ed.).
Zhou, J.X., Huang, Z.L., Bao, G.P., Gao, J.G., 2013f. Sources and thermo-chemical sulfate reduction for reduced sulfur in the hydrothermal fluids, southeastern SYG Pb–Zn metallogenic province, SW China. J. Earth Sci. 24, 759–771.
Zhou, J.X., Huang, Z.L., Zhou, M.F., Zhu, X.K., Muchez, P., 2014a. Zinc, sulfur and lead isotopic variations in carbonate-hosted Pb–Zn sulfide deposits, southwest China. Ore Geol. Rev. 58, 41–54.
Zhou, J.X., Huang, Z.L., Lv, Z.C., Zhu, X.K., Gao, J.G., Mirnejad, H., 2014b. Geology, isotope geochemistry and ore genesis of the Shanshulin carbonate-hosted Pb–Zn deposit, southwest China. Ore Geol. Rev. 63, 209–225.
Zhou, J.X., Bai, J.H., Huang, Z.L., Zhu, D., Yan, Z.F., Lv, Z.C., 2015. Geology, isotope geochemistry and geochronology of the Jinshachang carbonate-hosted Pb–Zn deposit, South China. J. Asian Earth Sci. 98, 272–284.
Zhou, J.X., Dou, S., Huang, Z.L., Cui, Y.L., Ye, L., Li, B., Gan, T., Sun, H.R., 2016. Origin of the Luping Pb deposit in the Beiya area, Yunnan Province, SW China: constraints from geology, isotope geochemistry and geochronology. Ore Geol. Rev. 72, 179–190.
Zhou, M.F., Malpas, J., Song, X.Y., Kennedy, A.K., Robinson, P.T., Sun, M., Lesher, M., Keays, R.R., 2002. A temporal link between the Emeishan large igneous province (SW China) and the end-Guadalupian mass extinction. Earth Planet. Sci. Lett. 196, 113–122.
Zhu, X.K., Guo, Y., Williams, R.J.P., O'Nions, R.K., Matthews, A., Belshaw, N.S., Canters, G.W., Waal, E.C.D., Weser, U., Burgess, B.K., Salvato, B., 2002. Mass fractionation processes of transition metal isotopes. Earth Planet. Sci. Lett. 200, 47–62.
Zhu, X.K., O'Nions, R.K., Guo, Y., Belshaw, N.S., Rickard, D., 2000. Determination of natural Cu isotope variation by plasmas source mass spectrometry: implications for use as geochemical tracers. Chem. Geol. 163, 139–149.